submitted to *Geophys. J. Int.*

Gravity Degree-Depth Relationship Using Point Mass Spherical Harmonics

Sander Goossens[1] and David E. Smith[2]

[1] *Planetary Geology, Geophysics, and Geochemistry Laboratory, NASA Goddard Space Flight Center, Greenbelt, MD 20771, USA. Email: sander.j.goossens@nasa.gov*

[2] *Department of Earth, Atmospheric and Planetary Sciences, Massachusetts Institute of Technology, Cambridge, MA 02139, USA. Email: smithde@mit.edu*

9 January 2023

SUMMARY

Relationships between the degree of a spherical harmonic model of the gravitational field of a body and the depth of a source expressed as a density contrast can be used to study the structure of features. Here, we show that the gravitational acceleration per spherical harmonic degree of a constant density source has an extremum that depends on the depth of the source. Using the spherical harmonics expansion for a point mass source, we use this to derive a degree-depth relationship. Our relationship resembles an earlier one derived by Bowin (1983), with substantial differences at the lower degrees. We also find that a recent relationship derived by Deng et al. (2022) over-estimates the source depth. The relationship that we derive relates spherical harmonic degree n to depth d for a planet of radius R according to $d = (1 - e^{\frac{-1}{n+1}})R$, which simplifies to $d = R/(n+1)$ for high degrees. We support our new relationship with synthetic models of a density contrast in a planet. We also show how the differences between our relationship and that of Bowin (1983) affect band-filtered gravity, for example when inspecting the upper 100 km of the Moon. Using point masses in our modeling results in an approximate relationship where in reality sources can be deeper than estimated, since any source contributes to all spherical harmonic degrees. The use of the contribution per individual degree however provides an intuitive relationship between spherical harmonic degree and depth that can be used to place relative bounds on source depths or to determine the bounds on spherical harmonic expansions when band-filtering gravity field models.

Key words: Geopotential theory – Planetary interiors – Satellite gravity.

1 INTRODUCTION

The gravity field of a planetary body is naturally expressed as a series expansion of spherical harmonics of a maximum degree and order. Interpretation of this field in terms of the internal density is inherently non-unique (*e.g.*, Blakely, 1995), however, expressions that relate spherical harmonic degree to source depth exist. Such expressions are at best an approximation due to the non-uniqueness. Gravitational quantities that can be measured (or determined from measurements), such as anomalies or geoid undulations (for definitions of quantities we refer to Section 2), can be related to the internal density distribution, resulting in the use of kernels or Green's functions that relate the two (*e.g.*, Blakely, 1995; Martinec, 2014). Such kernels, when expressed in spherical harmonics, can establish the sensitivity of sources at depth to spherical harmonic degree. However, in general a unique relationship cannot be established because any source contributes to all the degrees (*e.g.*, Bowin, 2000). To truly resolve density from gravity, one thus has to resort to inversion methods with the use of additional constraints, data, or both.

Under simplifying assumptions however, relationships between degree and depth can be established. While approximations, these can be useful, for example to place relative bounds on sources inside the planet, or to establish bounds when band-filtering a gravity field model with the goal to isolate signals related to depth. Here we focus on such relationships, while we acknowledge that there are more complete methods, with the addition of other data and assumptions, to determine density from gravity.

We identified two relationships in literature that we will introduce here. Bowin (1983, 1986) presented the following relationship between spherical harmonic degree n and depth d for a planet

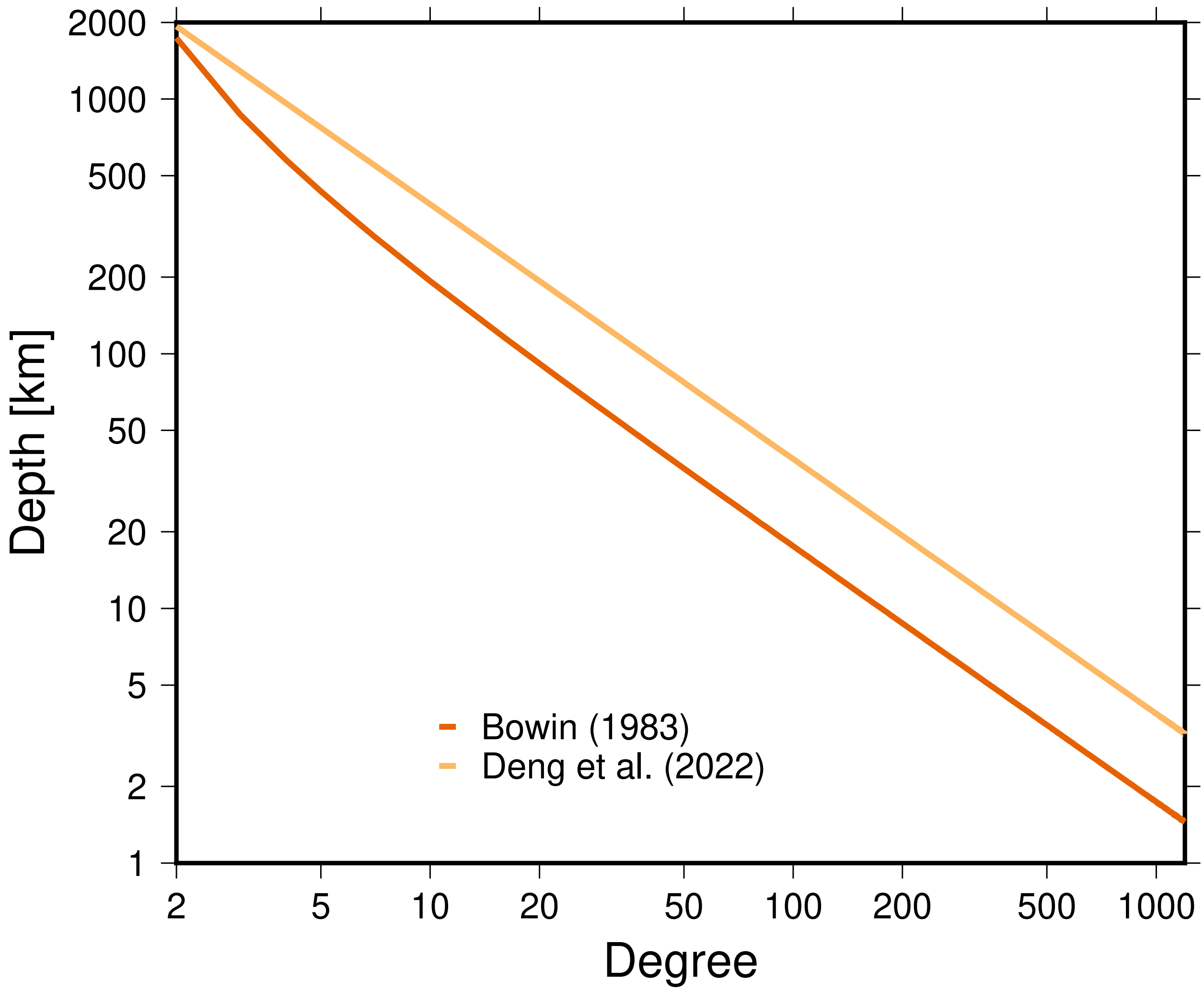

Figure 1. Degree-depth relationships from Bowin (1983) and Deng et al. (2022) for a planet with the Moon's radius (1738 km). Note that both axes have logarithmic scales.

of radius R,

$$d = \frac{R}{n-1}. \tag{1}$$

This relationship has been used in Earth and planetary applications; for example, to place constraints on the internal mass anomaly distribution in the Earth, and to filter gravity field quantities such as anomalies and geoid when investigating the structure of local features on the Earth and terrestrial planets. More recently, Deng et al. (2022) derived a different relationship,

$$d = \frac{\pi R}{\sqrt{2}n}. \tag{2}$$

It is obvious that these two relationships do not agree (see Figure 1). At degree $n = 2$, Bowin (1983) suggests a depth equal to the radius R, whereas the relationship from Deng et al. (2022)

suggests a depth larger than the planet's radius, because $\pi/(2\sqrt{2}) > 1$. This may suggest that equation (2) is only valid for large n, but this is not explicitly stated.

Here, we revisit simplified degree-depth relationships, by considering the gravitational potential of a point mass expressed in spherical harmonics, following Pollack (1973) and Sutton et al. (1991). Point masses are extremes resulting in approximate relationships, but they are useful as more complex mass anomalies can be represented as a group of point masses. We show that the gravitational acceleration of a point mass per spherical harmonic degree has an extremum, and this can be used to establish a degree-depth relationship.

This paper is structured as follows. We introduce the necessary quantities in Section 2. In Section 3 we introduce the spherical harmonics for a point mass, and show that the gravitational acceleration per degree has an extremum. We use this to derive a degree-depth relationship. We compare this new relationship to the existing ones in Section 4, and we show that an adjustment in the derivation by Bowin (1983) results in a close match with our relationship at high degrees. We test our degree-depth relationship in synthetic test cases in Section 5, where we estimate the depth of a density anomaly from spherical harmonics obtained through numerical integration. In Section 6 we discuss the advantages and limitations of simplified relationships, and we show an example of how the different relationships may result in different interpretations of features on the Moon, using a recent lunar gravity field model. We end with our conclusions in Section 7.

2 PRELIMINARIES

We introduce definitions and quantities that we will use in the remainder of this paper. These are standard expressions and relations which can be found in many textbooks; we mostly used Jekeli (2007).

The general expression for the gravitational potential $V(Q)$ of a body at a point $Q(r, \lambda, \theta)$ is

$$V(Q) = G \iiint_{\Omega} \frac{\rho(\Omega)}{\ell(Q, \Omega)} d\Omega, \tag{3}$$

with G the gravitational constant, Ω the volume of the body, $d\Omega$ the volume element, and $\ell(Q, \Omega)$ the distance between the point Q where the potential has to be computed and a point inside the body. The point Q is expressed in spherical coordinates with r the distance, λ the longitude, and θ the co-latitude. The density $\rho(\Omega)$ is indicated as varying within the volume, hence the dependency on Ω.

The gravity potential W is defined as the sum of the gravitational potential V and the rotational (or centrifugal) potential $\Phi = \frac{\omega^2}{2}(x^2 + y^2)$, where ω is the angular velocity and the Cartesian coordinates x and y are squared to provide the distance to the rotational axis. It is convenient to introduce the disturbing potential, $T = W - U$, where U is the normal potential, defined as the potential of a reference ellipsoid, and it includes the rotational potential. We will use the disturbing potential T in the remainder of this work.

The standard expression for $V(Q)$ in spherical harmonics reads

$$V(Q) = \frac{GM}{R} \sum_{n=0}^{\infty} \sum_{m=-n}^{m=n} \left(\frac{R}{r}\right)^{n+1} \bar{v}_{nm} \bar{Y}_{nm}(\theta, \lambda), \tag{4}$$

where GM is the gravitational parameter of the planet with mass M, and R is the reference radius. The function $\bar{Y}_{nm}(\theta, \lambda)$ is defined as

$$\bar{Y}_{nm}(\theta, \lambda) = \bar{P}_{n|m|}(\cos\theta) \begin{cases} \cos m\lambda, \ m \geq 0 \\ \\ \sin |m|\lambda, \ m < 0 \end{cases}, \tag{5}$$

with $\bar{P}_{nm}(\cos\theta)$ the associated Legendre functions of degree n and order m. The bar indicates normalization of these functions, and we use the 4π normalization that is standard in geodesy and geophysics (see also Wieczorek (2015)). Coefficients $\bar{v}_{nm}$ in equation (4) represent the standard gravity field model coefficients $\bar{C}_{nm}$ (when $m \geq 0$) and $\bar{S}_{nm}$ (when $m < 0$). A similar expression as equation (4) can be used for T with coefficients $\delta\bar{v}_{nm}$, which are the difference in coefficients between the total and reference (normal) potential. Here, we will assume a spherical approximation, which means that the normal potential will be that of a sphere of uniform density; all its coefficients (except $\bar{C}_{00}$ which represents the central term) will be zero, and the coefficients for the disturbing potential effectively become those of the potential V; we will thus drop the δ for $\delta\bar{v}_{nm}$.

There are a few relationships using Legendre functions that are useful for this work. First, the inverse of the distance between two points $P(r', \lambda', \theta')$ and $Q(r, \lambda, \theta)$ can be expressed in Legendre functions as

$$\frac{1}{\ell(P,Q)} = \frac{1}{r'} \sum_{n=0}^{\infty} \left(\frac{r'}{r}\right)^{n+1} P_n(\cos\psi);\ r > r', \tag{6}$$

where r' and r are radial distances to the two points (as noted, $r > r'$), and ψ is the angle between the two points. The function P_n is the unnormalized Legendre polynomial. It is also known that

$$P_n(\cos\psi) = \frac{1}{2n+1} \sum_{m=-n}^{m=n} \bar{Y}_{nm}(\theta,\lambda)\ \bar{Y}_{nm}(\theta',\lambda'). \tag{7}$$

We can thus use equation (7) in equation (6), and rewrite equation (3) as

$$\begin{aligned} V &= G \iiint_{\Omega} \rho(\Omega) \frac{1}{r'} \sum_{n=0}^{\infty} \left(\frac{r'}{r}\right)^{n+1} \frac{1}{2n+1} \sum_{m=-n}^{m=n} \bar{Y}_{nm}(\theta,\lambda) \bar{Y}_{nm}(\theta',\lambda')\ d\Omega \\ &= \sum_{n=0}^{\infty} \sum_{m=-n}^{m=n} \frac{G}{2n+1} \left(\frac{R}{r}\right)^{n+1} \left[\iiint_{\Omega} \rho(\Omega)(r')^n \frac{1}{R^{n+1}} \bar{Y}_{nm}(\theta',\lambda')\ d\Omega\right]\ \bar{Y}_{nm}(\theta,\lambda). \end{aligned} \tag{8}$$

By comparing equation (8) to equation (4), an expression for the coefficients $\bar{v}_{nm}$ depending on the internal density distribution can be obtained as

$$\bar{v}_{nm} = \frac{1}{M(2n+1)R^n} \iiint_{\Omega} \rho(\Omega)\ (r')^n \bar{Y}_{nm}(\theta',\lambda')\ d\Omega. \tag{9}$$

For clarity we repeat that these are also the coefficients for T since our reference gravity is a sphere of uniform density.

Additional quantities that are of use are derivatives of the potential T. The gravity disturbance δg is the difference between gravity (the gradient of the potential) and normal gravity, both evaluated at the same point, whereas the gravity anomaly Δg is the difference between gravity at a point and normal gravity on the reference surface (where the point on the reference surface is such that the normal potential at that point equals the potential at the point where gravity is computed). We will call the disturbance *(radial) acceleration* in the remainder. In spherical approximation, these quantities can be expressed in terms of T following

$$\delta g = -\frac{\partial T}{\partial r}, \tag{10}$$

$$\Delta g = -\frac{\partial T}{\partial r} - 2\frac{T}{r}. \tag{11}$$

Using the spherical harmonics expression for T following equation (4) these can also be expressed as

$$\delta g = \frac{GM}{r^2} \sum_{n=0}^{\infty} (n+1) \left(\frac{R}{r}\right)^n \sum_{m=-n}^{n} \bar{v}_{nm} \bar{Y}_{nm}(\theta, \lambda), \tag{12}$$

$$\Delta g = \frac{GM}{r^2} \sum_{n=0}^{\infty} (n-1) \left(\frac{R}{r}\right)^n \sum_{m=-n}^{n} \bar{v}_{nm} \bar{Y}_{nm}(\theta, \lambda). \tag{13}$$

The difference between the anomaly and acceleration is the factor depending on degree, which is $(n-1)$ for anomalies and $(n+1)$ for accelerations. We refer to Li & Götze (2001) and Hackney & Featherstone (2003) for additional discussions of the disturbance (acceleration) and anomaly.

3 POINT MASS SPHERICAL HARMONICS

Pollack (1973) and Sutton et al. (1991) discuss spherical harmonic expressions for discrete mass elements, including a point mass, spherical cap, and spherical rectangle. In the case of Pollack (1973) the mass elements are two-dimensional (surface elements) located at the reference surface, whereas Sutton et al. (1991) extend this to 3-D analogues at any depth. The point mass results of Pollack (1973) and Sutton et al. (1991) are readily derived.

The disturbing potential $T(Q)$ at point Q of a point mass located at point P is defined as

$$T(Q) = \frac{GM}{\ell(P, Q)}. \tag{14}$$

Following Sutton et al. (1991) we use the term disturbing potential here, as the masses are considered disturbing elements. Using equation (6), this can also be expressed as

$$T(Q) = \frac{GM}{r} \sum_{n=0}^{\infty} \left(\frac{r'}{r}\right)^n P_n(\cos\psi). \tag{15}$$

In addition, using equation (7) in equation (15) provides an equation for the potential of a point mass in the form of the general spherical harmonics expression equation (4), and in this way we can obtain an expression for the coefficients $\bar{v}_{nm}$ (or, $\bar{C}_{nm}$ and $\bar{S}_{nm}$) of a point mass, which is

$$\bar{v}_{nm} = \frac{1}{2n+1} \left(\frac{r'}{R}\right)^n \bar{Y}_{nm}(\theta', \lambda'). \tag{16}$$

Next, we inspect the radial accelerations, as these are often used in the geophysical analysis of gravity fields. We observed that the contribution of each separate spherical harmonic degree n to the gravitational acceleration has a maximum, and that this maximum shifts when the depth of the

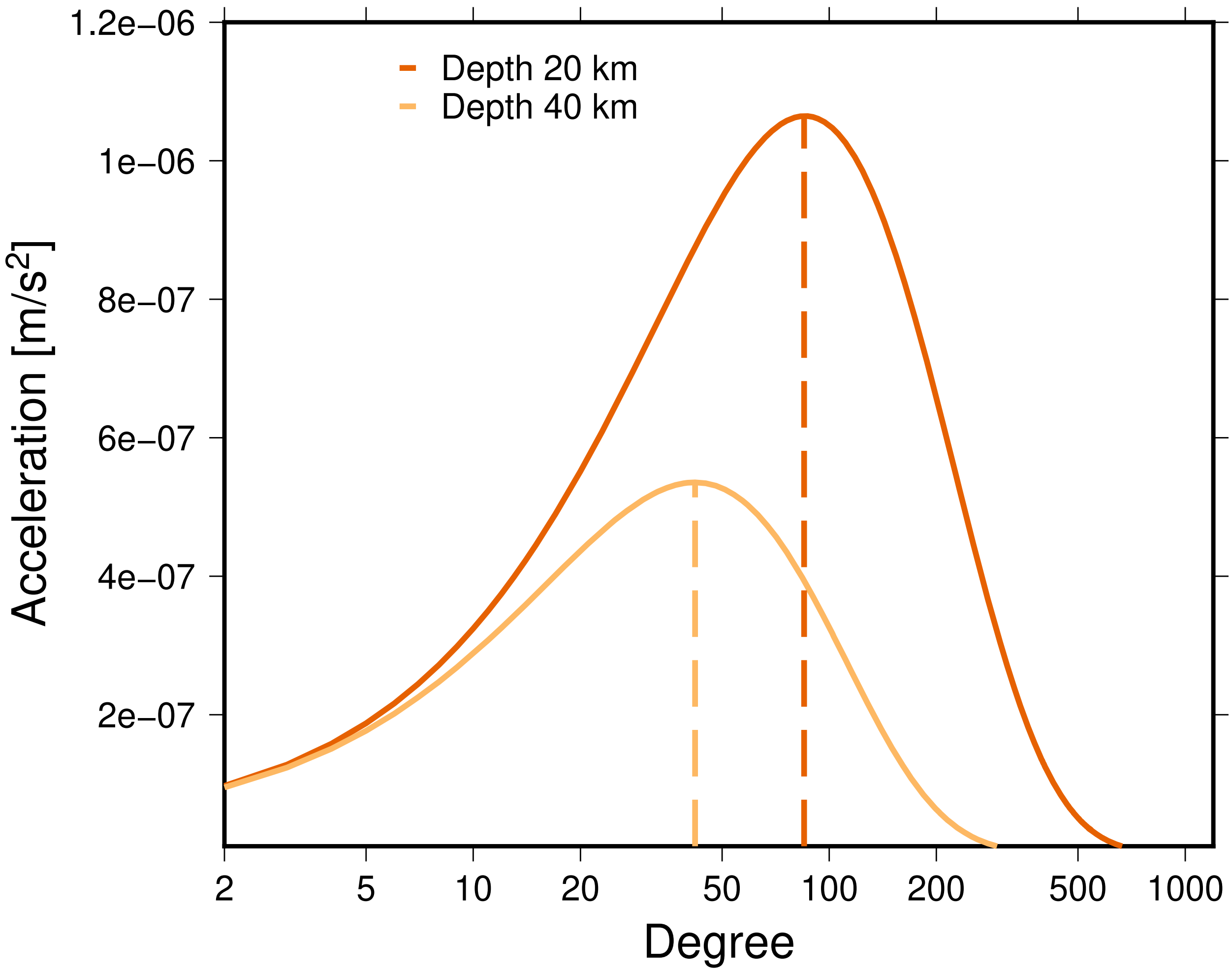

Figure 2. Gravitational acceleration for each spherical harmonic degree separately for point masses at a depth of 20 km or 40 km. The reference radius is 1738 km. The factor GM was conveniently set to 1. The point where the accelerations are computed is directly above the point mass, at the reference surface (depth is 0 km). The extremes for each depth are indicated with dashed lines.

source is changed. We illustrate this in Figure 2, where we plot accelerations for individual degrees for spherical harmonics expansions of point masses at a depth of 20 km or 40 km on a planet with the reference radius of the Moon (1738 km). We obtain these individual degree accelerations from equation (12), after computing the $\bar{v}_{nm}$ coefficients for each point mass source from equation (16). The degree at which the contribution reaches its maximum becomes smaller for larger depths. We thus inspect the expression for the radial acceleration of a point mass more closely to find this maximum.

Instead of using expressions for $\bar{v}_{nm}$, we directly use equation (15) to obtain the radial acceleration at a point Q as

$$\delta g(Q) = -\frac{\partial T(Q)}{\partial r} = \frac{GM}{r^2}\sum_{n=0}^{\infty}(n+1)\left(\frac{r'}{r}\right)^n P_n(\cos\psi). \tag{17}$$

This acceleration is the strongest directly above the point mass; in other words, for the case $\psi = 0°$ ($\theta' = \theta$ and $\lambda' = \lambda$) and thus $\cos\psi = 1$. We further note that the Legendre functions $P_n(\cos\psi)$ are standardized such that $P_n(1) = 1$ (these are still the *unnormalized* Legendre functions), which means that there is no additional degree dependency coming from $P_n(\cos\psi)$ for an expression of the acceleration directly above the point mass. This also means that the radial acceleration at $\tilde{Q}(r, \lambda', \theta')$ due to a point mass at $P(r', \lambda', \theta')$ is expressed as

$$\delta g(\tilde{Q}) = -\frac{\partial T(\tilde{Q})}{\partial r} = \frac{GM}{r^2}\sum_{n=0}^{\infty}(n+1)\left(\frac{r'}{r}\right)^n. \tag{18}$$

For each degree n separately, the radial acceleration $\delta g(\tilde{Q})(n)$ then is

$$\delta g(\tilde{Q})(n) = \frac{GM}{r^2}(n+1)\left(\frac{r'}{r}\right)^n. \tag{19}$$

The driving factor for the acceleration is the function

$$q(r', n) = (n+1)\left(\frac{r'}{r}\right)^n, \tag{20}$$

were we note that the point $\tilde{Q}$ at distance r will be fixed; hence we leave out the additional factor GM/r^2 and make q dependent on r' and n. We can take the derivative of this function with respect to n to determine at which degree n for a given radius r' this function has a maximum.

$$\frac{\partial q(r', n)}{\partial n} = \left(\frac{r'}{r}\right)^n + (n+1)\ln(\frac{r'}{r})\left(\frac{r'}{r}\right)^n. \tag{21}$$

Setting this to zero results in

$$n = -\frac{1}{\ln(\frac{r'}{r})} - 1. \tag{22}$$

If furthermore we set the computation point to be on the reference sphere $r = R$ and let d be the depth such that $r' = R - d$, then we can find the degree where the individual acceleration per spherical harmonic degree has a maximum for a point mass at depth d from

$$n = -\frac{1}{\ln(1 - \frac{d}{R})} - 1. \tag{23}$$

Conversely, we can express d as a function of n following the form of equations (1) and (2), which results in

$$d = (1 - e^{\frac{-1}{n+1}})R. \tag{24}$$

This is our degree-depth relationship.

4 COMPARISON WITH OTHER DEGREE-DEPTH RELATIONS

In Figure 3A we compare the three relations. Our newly derived relationship matches that from Bowin (1983) at high degrees, but there is a considerable difference in the estimated depth at lower degrees (Figure 3B). Equation (1) was derived by inspecting the ratio of the geoid and gravity, and by comparing that to that of a point mass. The geoid height N can be obtained from Bruns' formula (*e.g.*, Jekeli, 2007),

$$N = \frac{T}{\gamma} \tag{25}$$

where γ is the normal gravity. In a spherical approximation normal gravity at the reference surface would be GM/R^2; in Bowin (1983) it is listed as a constant, g_0. This results in a spherical harmonic expression for the geoid,

$$N(r, \lambda, \theta) = \frac{GM}{rg_0} \sum_{n=0}^{\infty} \left(\frac{R}{r}\right)^n \sum_{m=-n}^{n} \bar{v}_{nm} \bar{Y}_{nm}(\theta, \lambda). \tag{26}$$

Bowin (1983) then uses equation (13) to express gravity; the spherical harmonics expression used by Bowin (1983) has a factor of $(n-1)$. Taking the ratio of equations (13) and (26) per degree results in

$$\frac{\Delta g_n}{N_n} = \frac{GM}{r^2} \frac{rg_0}{GM}(n-1) = \frac{g_0(n-1)}{r}. \tag{27}$$

For a point mass at depth d, the disturbing potential directly above it is $T = GM/d$, the geoid then is $N = T/g_0 = GM/(g_0 d)$, and gravity is $g = GM/d^2$. The ratio of gravity and geoid for a point mass then becomes

$$\frac{g}{N} = \frac{g_0}{d}. \tag{28}$$

By equating equation (27) and (28), and using the reference radius, $r = R$, the degree-depth relationship of equation (1) is obtained.

Bowin (1983) thus uses the expression for a gravity anomaly. We observe that if, instead, the

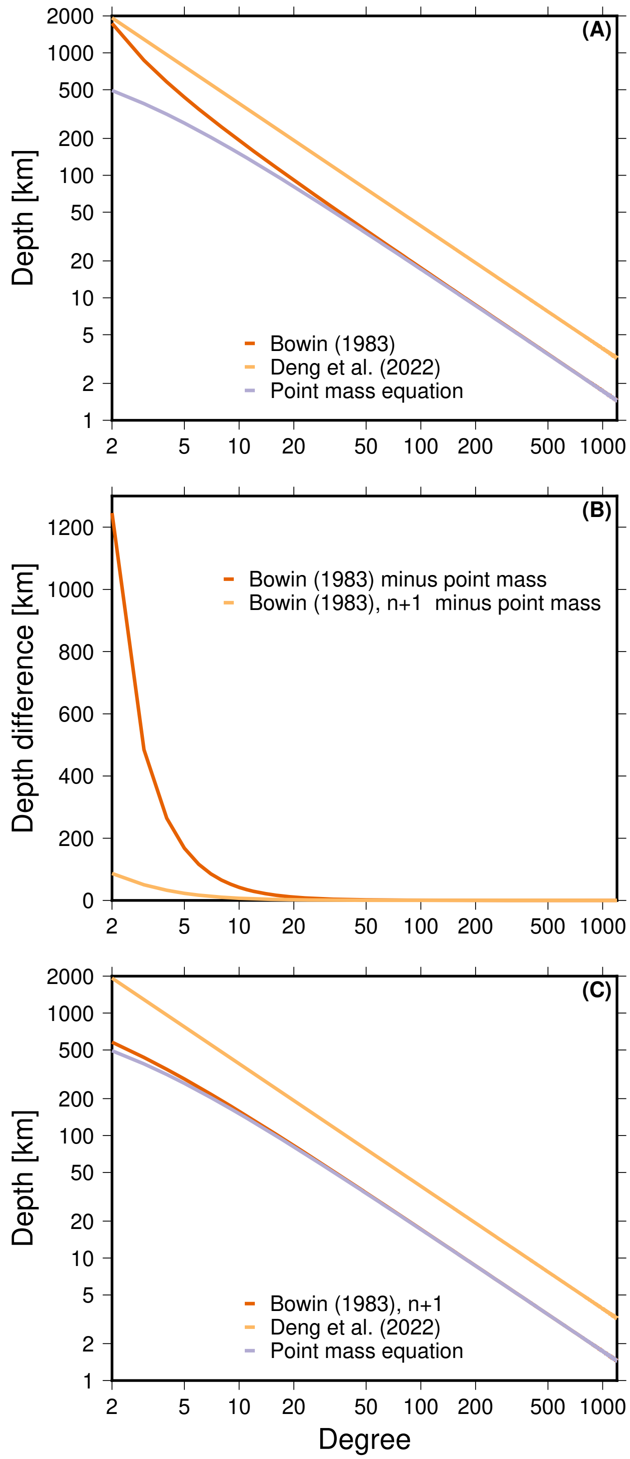

Figure 3. (top) Degree-depth relationships as in Figure 1, now also including our newly derived relationship from equation (24), labeled "Point mass equation". (middle) Difference in estimated depth between our relationship and that of Bowin (1983), including a modified version of Bowin (1983) which uses a factor of $(n+1)$ instead of $(n-1)$. See further explanations in the text. (bottom) The same as in the top plot, now including our modified version of Bowin (1983). The reference radius is again 1738 km.

radial acceleration as expressed in equation (12) is used, then the factor of $(n-1)$ in equation (27) is replaced with $(n+1)$ and the relation from equation (1) changes to

$$d = \frac{R}{n+1}. \tag{29}$$

We include this relation in Figure 3C, and we note that our modification of the relationship as presented by Bowin (1983) only affects interpretation of the lower degrees. Now there are only relatively small differences for the lowest degrees (see also Figure 3B). At degree $n = 2$ the difference is about 90 km, and at degree $n = 10$ it is only 7 km, whereas the differences with the relationship from equation (1) are much larger at the lower degrees. For that relationship, the differences at degree $n = 10$ are still 42 km, which is close to the average thickness of the lunar crust (Wieczorek et al., 2013).

The match at higher degrees between equations (23) and (29) can also be understood by considering the first order Taylor expansion

$$\ln(1+x) = x - \frac{x^2}{2} + \frac{x^3}{3} - \ldots \ . \tag{30}$$

With $x = -\frac{d}{R}$ and ignoring higher order terms for $\frac{d}{R} \ll 1$, the term $\ln(1-\frac{d}{R})$ in our expression becomes $-\frac{d}{R}$. Using this in equation (23) results in equation (29).

As Figure 3 indicates, there are still considerable differences between our relationship and that presented by Deng et al. (2022). They also considered a point mass and its decreasing gravitational effect, yet their relationship predicts larger depths for a given degree, and a depth larger than the planet's radius for degree $n = 2$. Deng et al. (2022) use the standard relationship to connect spherical harmonic wavelength to degree,

$$\lambda = \frac{2\pi R}{n}, \tag{31}$$

where often the half-wavelength is used to indicate spatial scales. Equation (31) however is an approximation. For example, Wieczorek (2015) notes that for a given spherical harmonic degree the equivalent Cartesian wavelength can be approximated as

$$\lambda \approx \frac{2\pi R}{\sqrt{n(n+1)}}, \tag{32}$$

which is called the Jeans relationship, following Jeans (1923). If this relationship is used, then, similar to equation (2), the new depth d_j would become

$$d_j = \frac{\pi R}{\sqrt{2n(n+1)}}. \tag{33}$$

In this case, for $n = 2$ the depth $d_j < R$ because $\pi/\sqrt{12} < 1$. For large n, the Jeans relation can be approximated as equation 31. This means that the relationship derived by Deng et al. (2022) is, strictly speaking, only valid for high degrees n. This is however not explicitly stated. But while this resolves the issue at degree $n = 2$, equations (2) and (33) are very similar (differences less than 10 km) for degrees $n >\sim 14$.

The derivations in Deng et al. (2022) also use a Cartesian geometry to derive the depth where the gravity signal vanishes. It can be questioned up to what degree or wavelength this is valid, and whether the surface curvature should be taken into account. For shallow depths however this would likely be less of an issue, and Figure 3 indicates there always is a factor (which is close to $\pi/\sqrt{2}$) of difference between their relationship and ours.

As mentioned, Deng et al. (2022) use the surface wavelength relationship of equation (31) to determine the depth at which the gravity signal vanishes. Yet it is not clear that the surface wavelength can readily be connected to a depth, even though it may seem intuitive (after all, surface wavelengths from spherical harmonics are often used as a rule of thumb to connect spacecraft altitude to the scales that are resolvable in a gravity field model; we note however that this always refers to scales, or resolution, at the surface). Our analysis does not use this assumption, but instead directly uses the spherical harmonics expansion of a point mass. As a result, the Legendre polynomials' surface wavelengths do not come into play, and this is the same for the relationship as derived in Bowin (1983).

5 TESTS WITH SYNTHETIC MODELS

In order to support our degree-depth relationship, we conduct two tests with synthetic models. For the first test, we determine the spherical harmonic coefficients for a block of 1 km by 1 km by 1 km with a density of 1000 kg m^{-3} at a depth of 50 km in a planet with the Moon's radius. We obtain the coefficients by means of numerical integration over the volume element, using equation

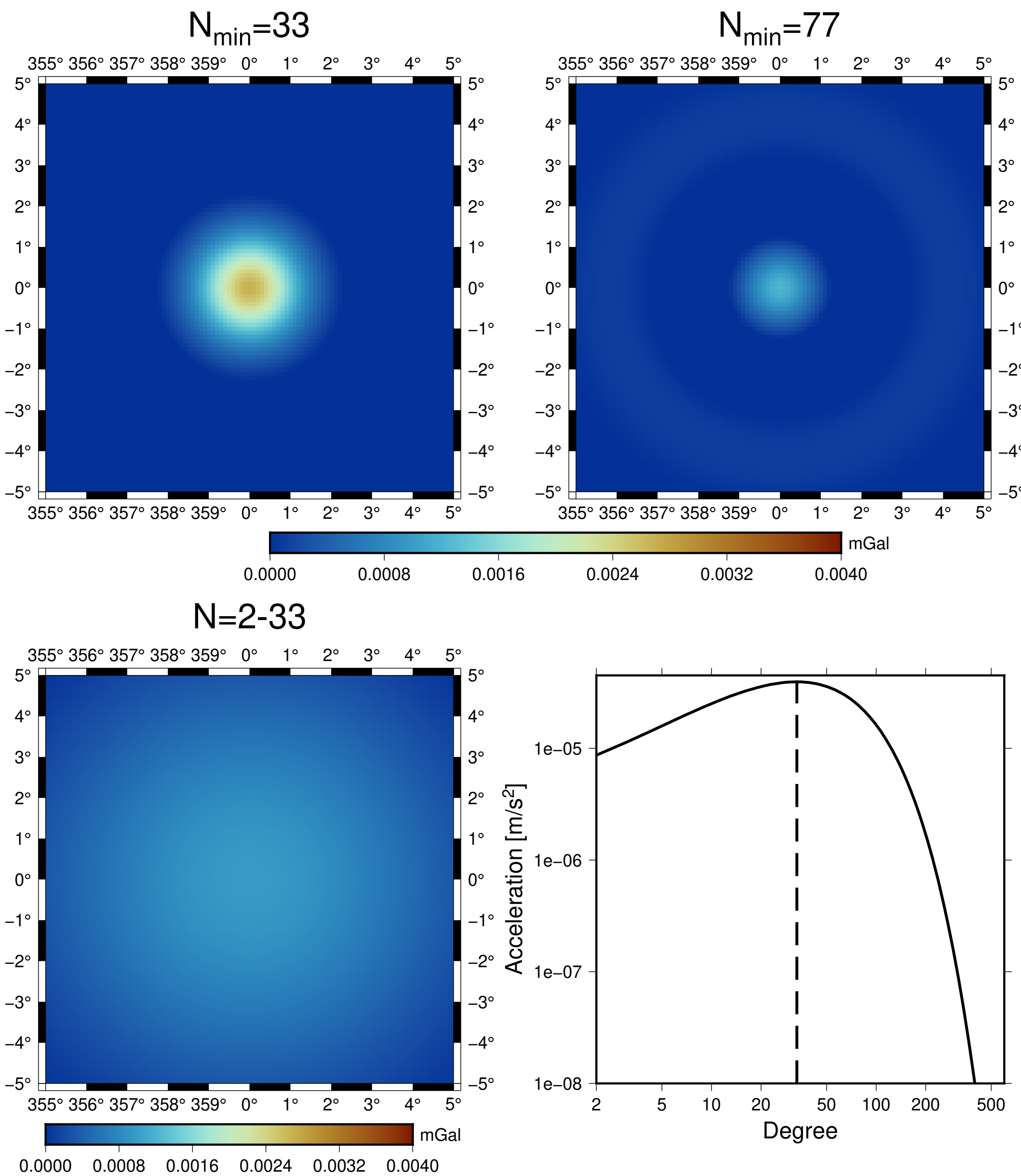

Figure 4. Gravity accelerations from the spherical harmonic expansion of a block of constant density of 1 by 1 by 1 km at 50 km depth on a planet with the Moon's radius with a density of 1000 kg m^{-3}. (top left) accelerations computed by band-filtering the spherical harmonics between $n = 33 - 600$; (top right) accelerations between $n = 77 - 600$; (bottom left) accelerations between $n = 2 - 33$; (bottom right) accelerations per individual degree, evaluated directly above the block at the reference surface. The maximum is indicated with a dashed line.

(9) with bounds for such an element. The maximum degree and order that we determine for this model is $n_{\max} = 600$. We note that Sutton et al. (1991) has expressions for a rectangular block as well. With the spherical harmonic coefficients for this block, we can band-filter the expression for gravity accelerations using equation (12).

In Figure 4 we show several acceleration maps, as well as the accelerations per individual degree. The latter are evaluated directly above the block, and all accelerations are computed at the reference surface. According to the relationship by Deng et al. (2022), a depth of 50 km corresponds to degree $n = 77$, whereas our relationship indicates $n = 33$. The latter can also be seen in the individual accelerations plot of Figure 4 (bottom right), which shows a peak at $n = 33$ (we note that the y-axis has a logarithmic scale). We now compute accelerations between different degree ranges: $n = 33 - 600$ (top left), $n = 77 - 600$ (top right), and $n = 2 - 33$ (bottom left).

Figure 4 shows that the accelerations when computed from $n = 33$ are stronger and more pronounced, whereas there is a much weaker signal for those starting at $n = 77$. The signal for degrees $n = 2 - 33$ is present, but also relatively weak. The idea behind band-filtering is to isolate signals, and to try to relate them to depth. According to the degree-depth relation from Deng et al. (2022), degrees $n = 77 - \infty$ (we cap them here at $n = 600$) should represent the upper 50 km of the planet, but the maps clearly show that there is more signal included in the lower degrees, from $n = 33$ on. According to the relationship from Deng et al. (2022) however, $n = 33$ would correspond to a depth of 117 km. This would either mean that the source would be placed deeper (when band-filtered from degree $n = 33$), or that part of the signal would be missed (when band-filtered from degree $n = 77$). We used a block rather than a point mass for this test, and note that for large enough distances from the block (compared to its size), it can be considered a point mass. Yet this test clearly indicates one would over-estimate the depth of the mass when using the relationship from Deng et al. (2022).

For the second test, we construct another mass inside a planet with the Moon's radius, this time with a larger volume. The mass is centered on a point with longitude 193.3°E and latitude 80.75°S, spanning depths down to 40 km. The central location and extent of the area cover the proposed Schrödinger-Zeeman basin (Neumann et al., 2015), but we stress that this model is a purely synthetic one, and the results do not depend on this specific location. The mass further consists of blocks of size 2/3° by 2/3° in latitude and longitude, and 5 km in the radial direction. With a depth of 40 km there are 8 layers and the extent of the area was chosen such that each layer has 54 blocks. The size for the blocks of 2/3° was chosen to have a surface wavelength that

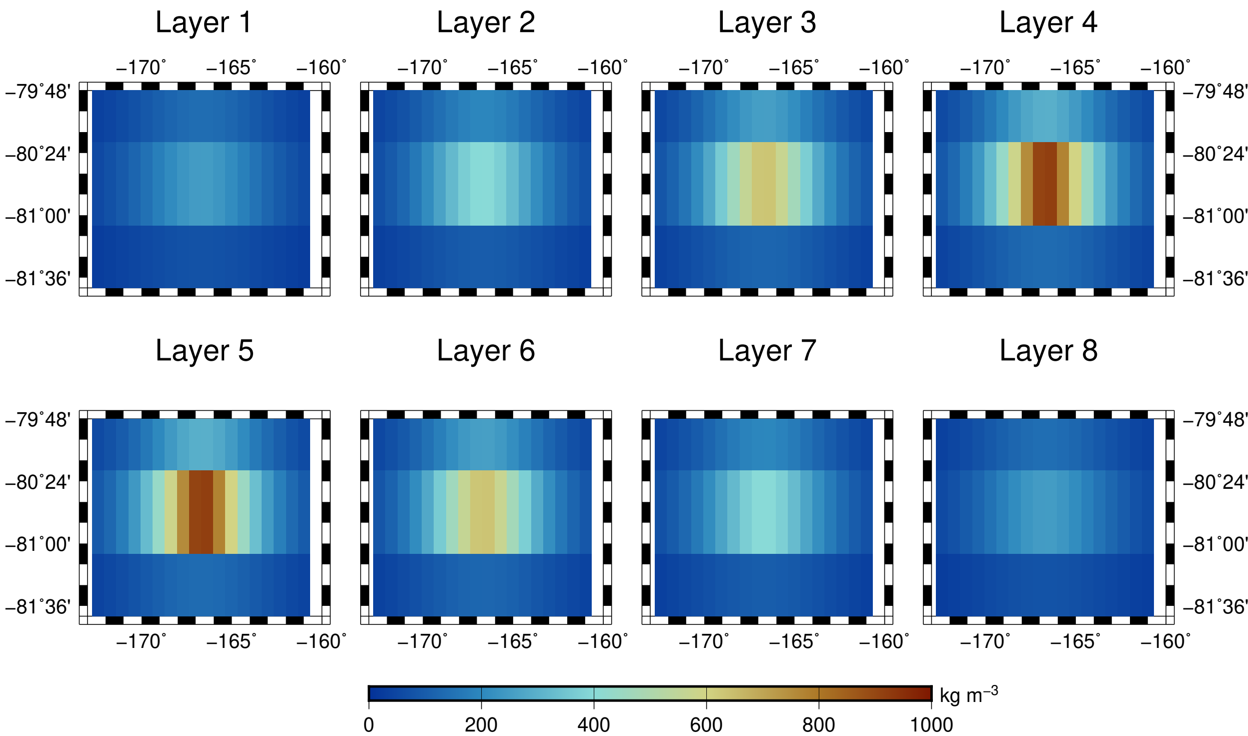

Figure 5. Density distribution for each 5 km thick layer, spanning from the surface to a depth of 40 km on a planet with the Moon's radius. Each layer has 54 density blocks of 2/3° by 2/3°. The blocks appear elongated because of the different ranges for longitude and latitude.

matches spherical harmonics degree 540 (equation (31)). We then create a varying density profile for this mass. We constructed a density distribution that decays exponentially, by choosing

$$\rho = \rho_0 \times e^{-r/D}, \tag{34}$$

where r is the distance of the center of a block to the center coordinates of the mass (193.3°E and 80.75°S at a depth of 20 km), D is a correlation distance that determines how quickly the density decreases and that we choose to be 10 km, and ρ_0 is the density scaling factor which we chose to be 1500 kg m^{-3}. This results in a spherically varying density that we depict for all 8 layers in Figure 5. This should be considered as a density contrast in the crust. We compute the spherical harmonic coefficients for this mass by numerical integration. In addition we also generate a gravity field model for a large mass of the same volume and location and of a constant density contrast of 150 kg m^{-3}.

We then compute the accelerations per spherical harmonic degree at the center point of the set of blocks, on the reference surface. We show these curves in Figure 6. The degree where the

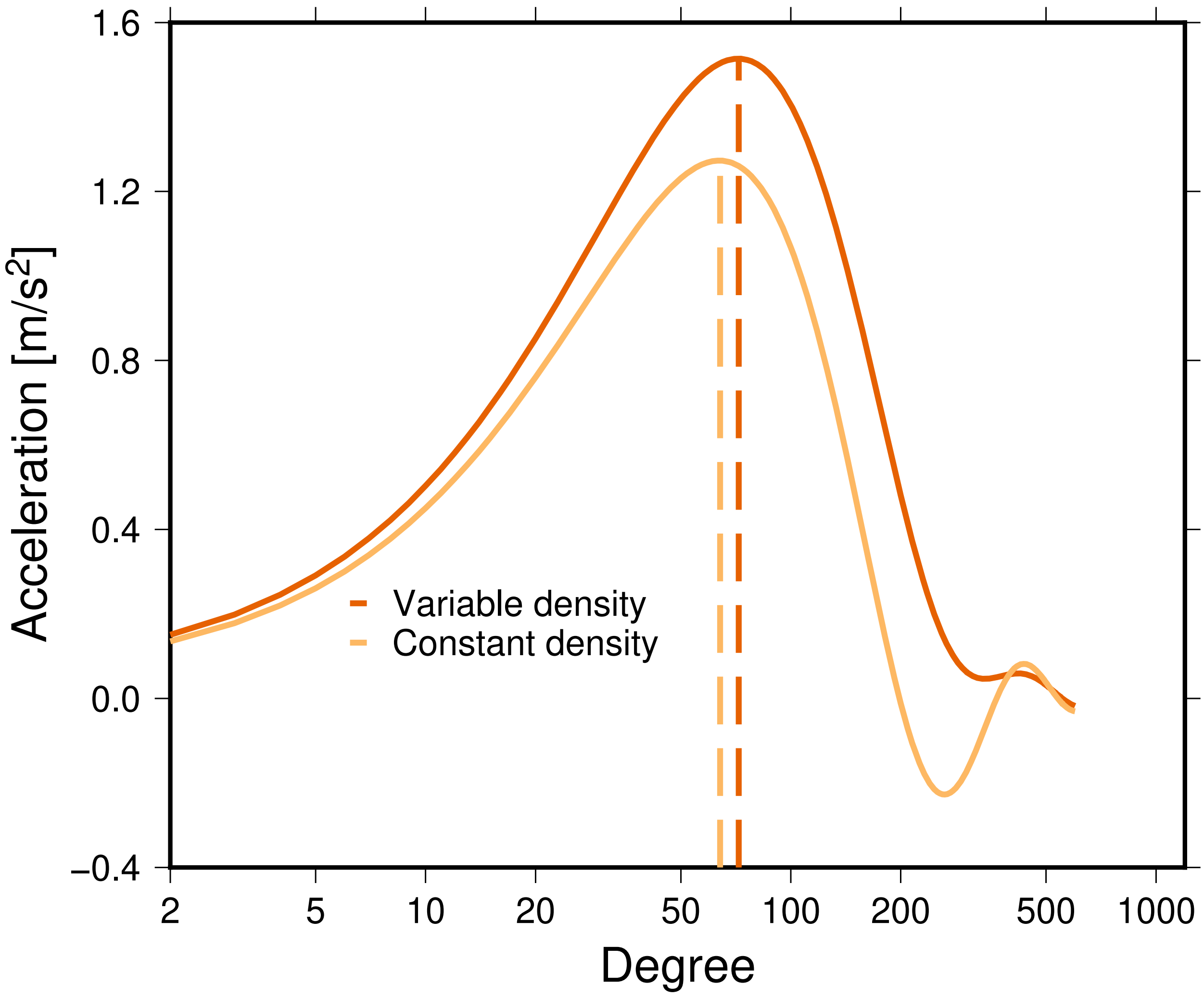

Figure 6. Gravitational acceleration for each spherical harmonic degree separately for the model of the gravity field caused by the density distribution as depicted in Figure 5 and for a block of the same size with a constant density. The point where the accelerations are computed is directly above the center point of the mass, at the reference surface. The extremes for each distribution are indicated with dashed lines

acceleration has a maximum is slightly different for the two curves, but they are close together: $n = 72$ for the case with varying density, and $n = 64$ for the case with constant density. The difference in maximum likely exists because of the density differences between the two cases. In the case of the constant density block, stronger density contrasts are present close to the surface. Using our degree-depth relationship, the maxima correspond to a depth of 23 km and 26 km, respectively. Using the relationship from Deng et al. (2022) the depths would be 53 km and 60 km, respectively. From Figure 5, the maximum density occurs in the center of the set of layers by design, and this is at a depth of 20 km. While not an exact match, our degree-depth relationship matches this closely.

6 DISCUSSION

The tests presented in the previous section support our degree-depth relationship. We specifically used blocks instead of point masses, and the tests with a large mass with varying or constant density was also sufficiently close to the surface that the blocks cannot be considered as point masses. Yet we recognize that all the masses in our tests have a positive density contrast, making them relatively simple structures.

The use of point masses in our analysis places limits on its usefulness. We thus compared our degree-depth relationship with results obtained through numerical integration. We placed blocks of different sizes (1 x 1 x 1 km, or 10 x 10 x 10 km) at various depths, determined their gravity field coefficients, and computed accelerations per individual degree directly above the block, at the reference surface. For each block at depth, we then determined the degree where the individual acceleration per degree has a maximum. We show the results in Figure 7, and they match our degree-depth relationship. Differences at the very low degrees are solely due to the fact that our numerical results will by definition always return an integer value for the degree where the acceleration per individual degree has a maximum, whereas our degree-depth relationship returns a real number for the degree for a given depth. This is most notable at the very low degrees. If for the sake of comparison we round the results for the degree from our relationship to have an integer value for a given depth, the match between the two is exact. While again blocks at depth can be considered point masses, this is not the case for the shallower blocks, yet the relationship holds.

Point masses can be considered extremes, with all mass concentrated in a single point, and this places limitations on their use for probing realistic structures. Yet they can provide bounds on the depth of sources, because using them as source models would indicate depths below which it is unlikely that the source originates (Dehlinger, 1978). Bowin (1991) also noted that the degree-depth relationship only works well for clearly defined anomalies. Masses with both large positive and negative density variations will show more complex accelerations at the surface, and one may

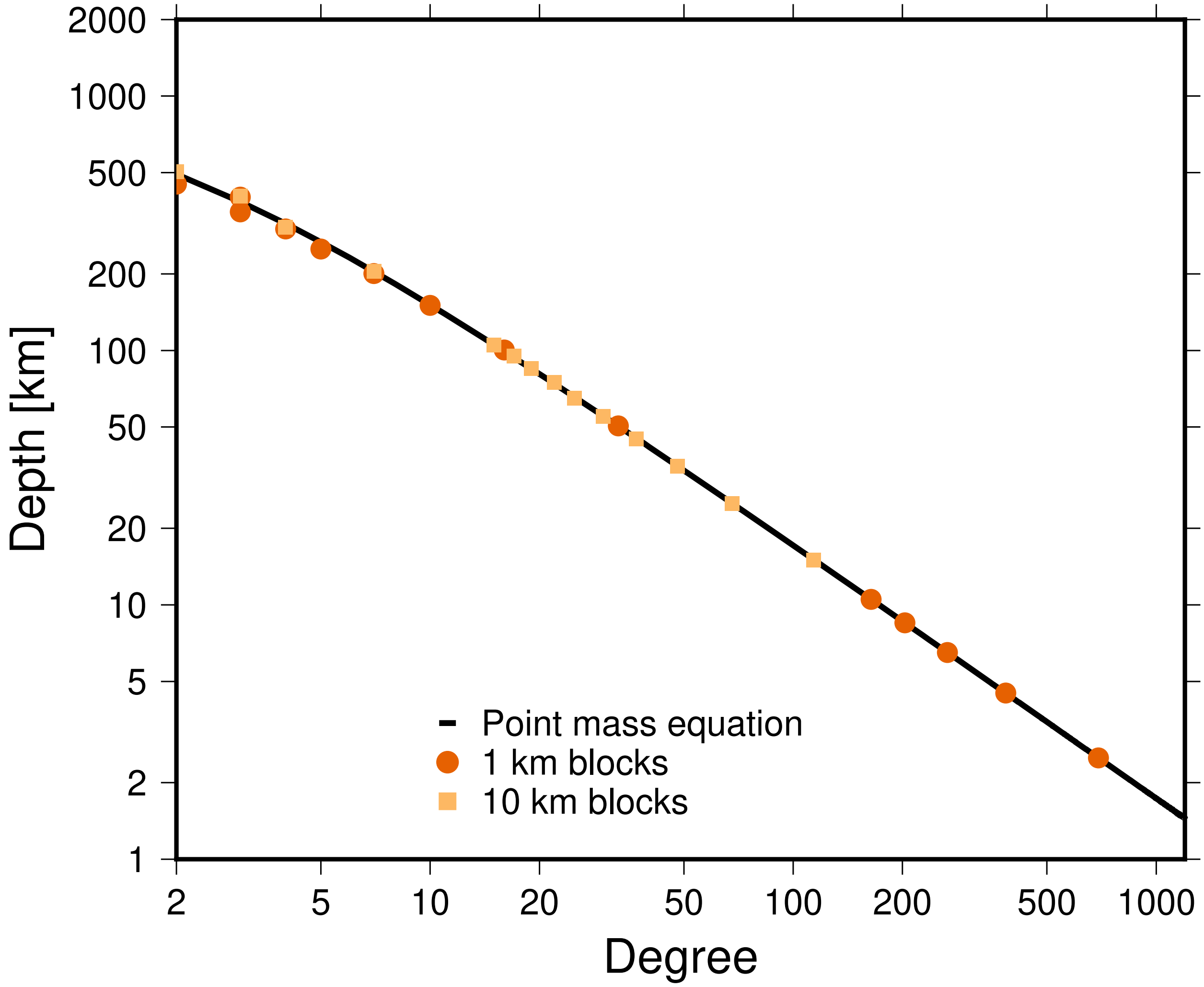

Figure 7. Degree at which accelerations computed per degree have a maximum, for blocks of different sizes (1 x 1 x 1 km or 10 x 10 x 10 km) at various depths. The density contrast for each block was 1000 kg m^{-3}. Gravity fields were computed by numerical integration, and the accelerations were computed directly above the blocks, at the reference surface. Our degree-depth relationship derived using point masses is also included.

need to revert to more direct inversions of gravity, which will require additional constraints and information to overcome the inherent non-uniqueness. Masses that are (isostatically) compensated would show no gravity signal at all. Yet the gravity fields of the Moon and Mars, and to a lesser extent Mercury (due to lower resolution) show plenty of craters with clearly defined negative or positive accelerations, or volcanic complexes with strong positive gravity accelerations. Degree-depth relationships like ours can then be used to place approximate bounds for the depth of the sources.

Our synthetic test determined the center depth of the feature very closely, but we did not probe the extent of the anomaly, which in this case was from the surface to 40 km. This indicates another limitation not necessarily of the point mass approach, but of assigning a depth to a degree. As mentioned in Section 1, any source contributes to all the spherical harmonic degrees. And while in our approach we focused on the maximum contribution because it results in a unique relationship between degree and depth, it is clear from Figure 2 that a wide range of degrees has a considerable contribution to the total accumulated acceleration. Sources can thus be deeper than our relationship indicates, even despite considering point masses as indicating some kind of maximum depth, as argued above (Dehlinger, 1978). In reality the structure will be more complicated. Yet these kind of relationships can give a good approximation of source depth; in our synthetic example it placed the concentrated mass close to where the actual center was.

We showed that our relationship resembles that of Bowin (1983), and it is thus fair to consider whether the differences are significant. At the lower degrees, there are considerable differences in estimated depth, as indicated in Figure 3B. It is interesting to note that Bowin (1991) indicated that the gravity-geoid ratio provides deeper point mass estimates than appropriate. Our relationship circumvents such an issue. In addition, the degree-depth relationship of Bowin (1983) has been used in Earth and planetary science to investigate band-limited representations of the accelerations, with the goal to place bounds on the depth extent of structures, or, alternatively, to investigate a certain region of the interior.

For example, to investigate the upper 100 km of the Moon, as Featherstone et al. (2013) did, the different degree-depth relationships result in different start degrees. Using the relationship of Bowin (1983) results in $n = 18$, that of Deng et al. (2022) in $n = 38$, and ours in $n = 15$. We show band-filtered Bouguer anomalies for the Moon in Figure 8, where Bouguer equals gravity from the lunar gravity field model GRGM1200B (Goossens et al., 2020) minus topography induced gravity (following Wieczorek & Phillips (1998), where we use a constant density for the lunar crust of 2500 kg m^{-3}). It is clear that following Deng et al. (2022), a lot of signal is not included, but it is difficult to imagine that most of the lunar mascon signal is below 100 km depth (*e.g.*, Melosh et al., 2013), which is what their relationship would yield when using a lower

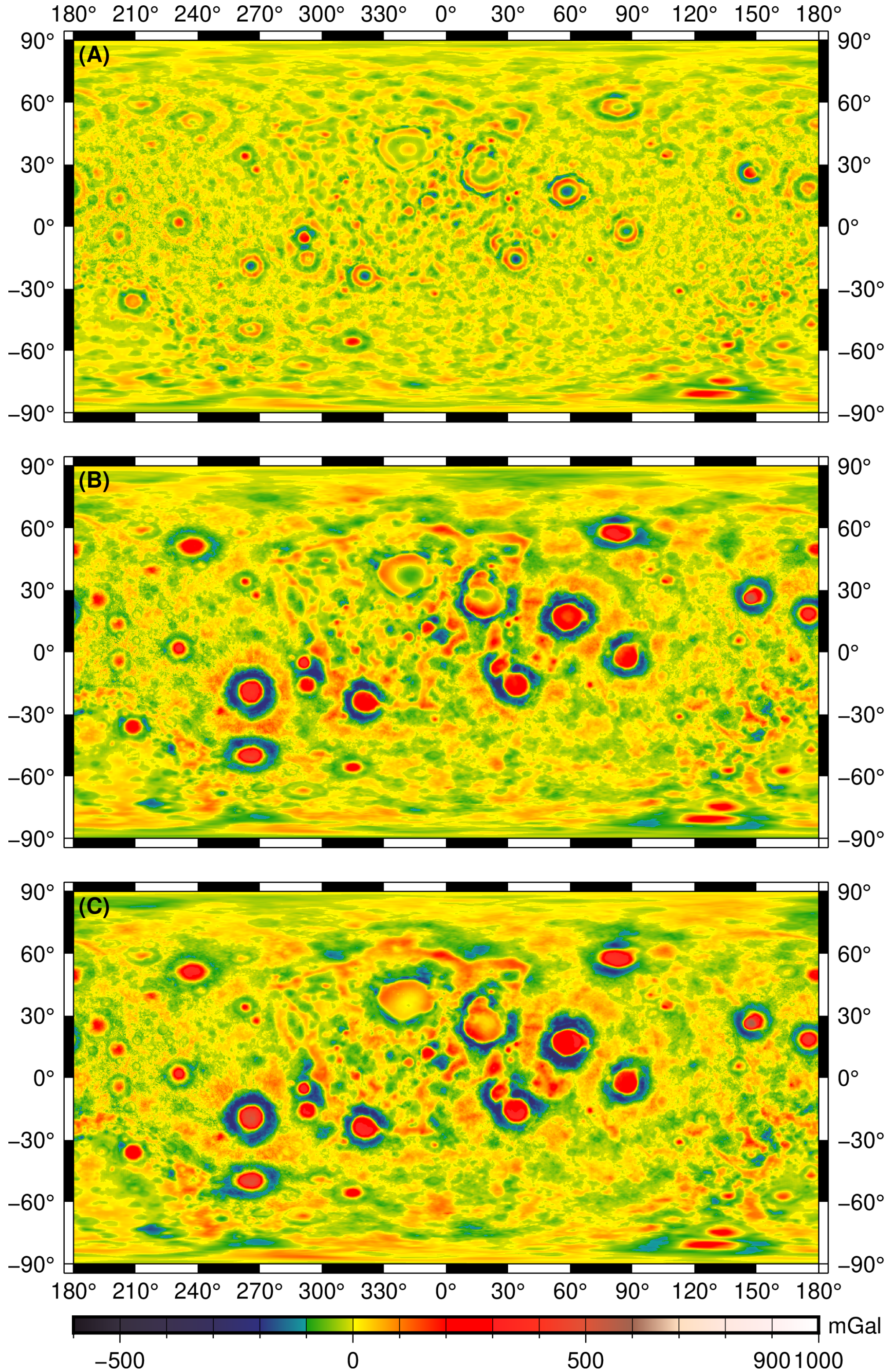

Figure 8. Band-filtered Bouguer anomalies for the lunar gravity field model GRGM1200B. Using different degree-depth relationships to show the upper 100 km of the lunar crust results in different start degrees: (top) $n = 38 - 540$, using Deng et al. (2022); (middle) $n = 18 - 540$, using Bowin (1983); (bottom) $n = 15 - 540$, using our relationship.

starting degree to include more of the central signal in the basins. The differences are of course smaller when comparing the results using Bowin (1983) and ours, yet especially some of the larger nearside mascons such as Imbrium (36°N, 342°E) or Serenitatis (26°N, 19°E) show differences in their interior, with the mascon using our relationship showing a more complete, positive signal at the center. This would make a difference also even if our relationship is not directly used to constrain source depth. If instead an inversion based on a sensitivity kernel were to be performed, the input signal would likely still be band-filtered based on source depth considerations, and the input signal would be different, missing some crucial signal in the interior of the large basins when using the relationship by Bowin (1983). Other features show less of a difference between these two band-filters, likely because they are shallower and so the cut-off for 100 km that was chosen here matters less. However, something similar occur if one were to focus on the upper 50 km.

In Section 4 we noted that Bowin (1983) used the gravity anomaly and not the gravity acceleration to derive his expression. While we used the expression for acceleration, equation (12), to derive our relationship, we observe that a degree-depth relationship can also be derived using the expression for the anomaly, equation (13). The derivation as given in equations (17) to (24) follows the same pattern, replacing the factor $(n + 1)$ with $(n - 1)$, resulting in a relationship

$$d = (1 - e^{\frac{-1}{n-1}})R, \tag{35}$$

which for large n would simplify to $d = R/(n - 1)$, exactly the same as that of Bowin (1983). We include this relationship in Figure 9, where we also show the differences in estimated depth with the expression from Bowin (1983), for both our relationship and the one based on the anomaly.

For this anomaly relationship, the differences with Bowin (1983) are smaller over all degrees, although it still results in several hundreds of km differences at the lowest degrees. The use of the geoid by Bowin (1983) may have resulted in a different depth-sensitivity: the expression for the geoid in spherical harmonics, equation (26), lacks multipliers of the degree n which means increased influence of lower degree terms because higher degrees are not as amplified as is the case for derivatives of the disturbing potential. Anomalies are related to the geoid, as discussed in Section 2. We note that using the expression for the geoid in spherical harmonics does not

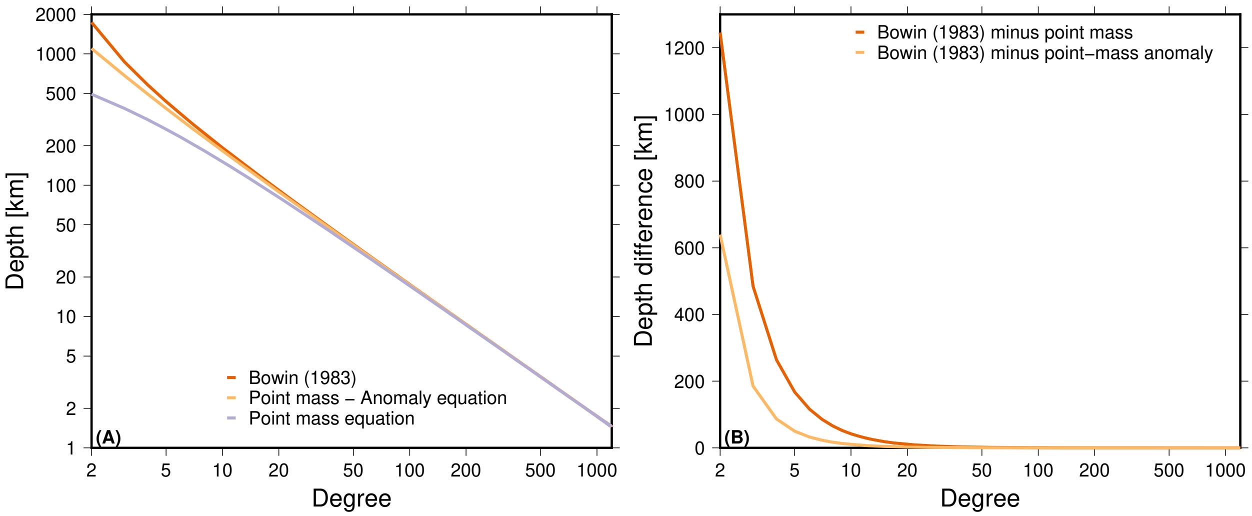

Figure 9. (left) Degree-depth relationships as before, also including our variation using the anomaly expression, labeled "Point mass - Anomaly equation". See further explanations in the text. (right) Differences in depth estimation between the expression from Bowin (1983) and our point mass equation, also including the differences between Bowin (1983) and our anomaly expression.

result in an extrema for the geoid contributions per degree, precisely because the expression lacks a multiplier of the degree n. The only function in the expression for the point mass geoid that is dependent on n would be the factor $(R/r)^n$ which is monotonically decreasing.

Ultimately, we find that the use of accelerations instead of the geoid is more intuitive for point masses: these accelerations are what is experienced (in the radial direction) by a spacecraft in orbit, and there is no additional reference to the geoid. While the ratio of anomaly and geoid results in a degree-depth relationship when compared to the acceleration of a point mass, but it mixes accelerations and anomalies and it is not clear to us what this ratio of geoid and anomaly represents. Our formulation in terms of the per degree contribution on the other hand clearly shows an extrema.

7 CONCLUSIONS

We presented a degree-depth relationship based on spherical harmonics for a point mass and on the observation that the contribution of separate spherical harmonic degrees to the radial acceleration has a maximum at a certain degree that depends on the depth. Our degree-depth relationship connects spherical harmonic degree n with depth d for a planet with radius R following

$$d = (1 - e^{\frac{-1}{n+1}})R.$$

We further demonstrated how our relationship compares to previously presented relationships. Our relationship resembles that of Bowin (1983) at high degrees, but there are substantial differences for the lower degrees. Bowin (1991) already indicated that the Bowin (1983) relationship resulted in deeper point mass estimates than appropriate. Our result avoids this. We explored the differences between the two relationships in more detail, and noted that a slight modification to the relationship of Bowin (1983) provides an even closer match to the one presented by us. This modified relationship is expressed as

$$d = \frac{R}{n+1},$$

and this matches our expression very closely, which can also be shown analytically for high degrees. Ultimately, our result obtained through the individual contribution per degree provides an intuitive framework to establish a clear relationship between depth and spherical harmonic degree.

Recently Deng et al. (2022) derived a different degree-depth relationship, which shows large differences with ours for all degrees. Their relationship uses the surface wavelength of the Legendre polynomials, as well as assumptions of Cartesian geometry, and it appears to be valid only for high degrees n (the latter implicitly). Our relationship is derived using point mass spherical harmonics expressions directly without the use of the surface wavelength. We hypothesize that this is the main cause for the difference between our relationships.

We supported our degree-depth relationship with two different synthetic tests, indicating that the relationship from Deng et al. (2022) over-estimates the depth of a structure. Our degree-depth relationship correctly indicated the depth of the structure. Our tests used straightforward structures, with only positive density contrasts. More complex structures with positive and negative density contrasts close together will be more difficult, yet planetary gravity fields have many clearly defined features.

The use of point mass expressions places limitations on the use of our relationship. While it can provide bounds on the depth of structures, as indicated by the results of our synthetic tests, it is possible that sources are located deeper, because any source contributes to all spherical harmonic degrees. An entirely unique relationship can thus not be established, and more elaborate methods will be required. Yet the simplification of considering point masses can be useful to provide approximate bounds for the relative depth of sources, or to provide bounds for band-filtering gravity when investigating, for example, only the upper parts of the planet. With an example using a lunar gravity field model, we showed how the different relationships result in different gravity maps. The relationship by Deng et al. (2022) would exclude a lot of signal; ours and that of Bowin (1983) have results that are closer, but in this example several of the larger basins on the Moon would still show an incomplete gravity signal in their center when using the relationship of Bowin (1983). Our relationship can thus be used to place bounds on structures, and to decide the bounds when studying band-filtered gravity accelerations.

DATA AVAILABILITY

The lunar gravity field model used in our example can be found at NASA's Planetary Data System, at `https://pds-geosciences.wustl.edu/grail/grail-l-lgrs-5-rdr-v1/grail_1001/shadr/gggrx_1200b_sha.tab`. The topography model needed to compute Bouguer gravity can also be found at the PDS at `https://pds-geosciences.wustl.edu/lro/lro-l-lola-3-rdr-v1/lrolol_1xxx/data/lola_shadr/pa/lro_ltm01_pa_1080_sha.tab`. Bouguer gravity can be computed using the freely available SHTOOLS software (Wieczorek et al., 2018).

ACKNOWLEDGMENTS

We would like to thank Dave Rowlands (NASA/GSFC) for the use of his numerical integration software. We thank Terry Sabaka (NASA/GSFC) and Maria Zuber (MIT) for discussions. We thank the editor, Prof. Juan Carlos Afonso, and two reviewers for their insightful comments. We made use of the freely available software SHTOOLS (Wieczorek et al., 2018). All figures were created with the freely available software GMT (Wessel et al., 2013).

References

Blakely, R., 1995. *Potential Theory in Gravity & Magnetic Applications*, Stanford - Cambridge Program, Cambridge University Press.

Bowin, C., 1983. Depth of principal mass anomalies contributing to the Earth's geoidal undulations and gravity anomalies, *Marine Geodesy*, **7**, 61–100.

Bowin, C., 1986. Depth estimates from ratios of gravity, geoid, and gravity gradient anomalies, *Geophysics*, **51**(1), 123.

Bowin, C., 1991. The Earth's gravity field and plate tectonics, *Tectonophysics*, **187**(1), 69–89.

Bowin, C., 2000. Mass anomaly structure of the Earth, *Reviews of Geophysics*, **38**(3), 355–388.

Dehlinger, P., 1978. *Marine gravity*, vol. 22 of **Elsevier Oceanography Series**, Elsevier Scientific Publishing Company, Amsterdam, The Netherlands.

Deng, Q., Li, F., Yan, J., Ye, M., & Barriot, J.-P., 2022. Degree-Depth Relation for Planetary Gravity Field Model Based on Wavelength, *Earth and Space Science*, **9**(5), e02143.

Featherstone, W. E., Hirt, C., & Kuhn, M., 2013. Band-limited Bouguer gravity identifies new basins on the Moon, *Journal of Geophysical Research (Planets)*, **118**(6), 1397–1413.

Goossens, S., Sabaka, T. J., Wieczorek, M. A., Neumann, G. A., Mazarico, E., Lemoine, F. G., Nicholas, J. B., Smith, D. E., & Zuber, M. T., 2020. High-resolution gravity field models from GRAIL data and implications for models of the density structure of the Moon's crust, *Journal of Geophysical Research: Planets*, **125**, e2019JE006086.

Hackney, R. & Featherstone, W., 2003. Geodetic versus geophysical perspectives of the 'gravity anomaly', *Geophysical Journal International*, **154**, 35–43.

Jeans, J. H., 1923. The Propagation of Earthquake Waves, *Proceedings of the Royal Society of London Series A*, **102**(718), 554–574.

Jekeli, C., 2007. Potential Theory and Static Gravity Field of the Earth, in *Geodesy, Treatise on Geophysics*, vol. 3, pp. 11–42, ed. Schubert, G., Elsevier.

Li, X. & Götze, H.-J., 2001. Tutorial: Ellipsoid, geoid, gravity, geodesy and geophysics, *Geophysics*, **66**(6), 1660–1668.

Martinec, Z., 2014. Mass-density Green's functions for the gravitational gradient tensor at different heights, *Geophysical Journal International*, **196**(3), 1455–1465.

Melosh, H. J., Freed, A. M., Johnson, B. C., Blair, D. M., Andrews-Hanna, J. C., Neumann, G. A., Phillips, R. J., Smith, D. E., Solomon, S. C., Wieczorek, M. A., & Zuber, M. T., 2013. The Origin of Lunar Mascon Basins, *Science*, **340**, 1552–1555, doi:10.1126/science.1235768.

Neumann, G. A., Zuber, M. T., Wieczorek, M. A., Head, J. W., Baker, D. M. H., Solomon, S. C., Smith, D. E., Lemoine, F. G., Mazarico, E., Sabaka, T. J., Goossens, S. J., Melosh, H. J., Phillips, R. J., Asmar, S. W., Konopliv, A. S., Williams, J. G., Sori, M. M., Soderblom, J. M., Miljković, K., Andrews-Hanna, J. C., Nimmo, F., & Kiefer, W. S., 2015. Lunar impact basins revealed by Gravity Recovery and Interior Laboratory measurements, *Science Advances*, **1**(9).

Pollack, H. N., 1973. Spherical harmonic representation of the gravitational potential of a point mass, a spherical cap, and a spherical rectangle., *Journal of Geophysical Research*, **78**, 1760–1768.

Sutton, S. T., Pollack, H. N., & Jackson, M. J., 1991. Spherical harmonic representation of the gravitational potential of discrete spherical mass elements, *Geophysical Journal International*, **107**(1), 77–82.

Wessel, P., Smith, W. H. F., Scharroo, R., Luis, J., & Wobbe, F., 2013. Generic Mapping Tools: Improved Version Released, *EOS, Transactions American Geophysical Union*, **94**(45), 409–410.

Wieczorek, M. A., 2015. Gravity and Topography of the Terrestrial Planets, in *Treatise on Geophysics (Second Edition)*, pp. 153–193, ed. Schubert, G., Elsevier, Oxford.

Wieczorek, M. A. & Phillips, R. J., 1998. Potential anomalies on a sphere: Applications to the thickness of the lunar crust, *Journal of Geophysical Research*, **103**(E1), 1715–1724.

Wieczorek, M. A., Neumann, G. A., Nimmo, F., Kiefer, W. S., Taylor, G. J., Melosh, H. J., Phillips, R. J., Solomon, S. C., Andrews-Hanna, J. C., Asmar, S. W., Konopliv, A. S., Lemoine, F. G., Smith, D. E., Watkins, M. M., Williams, J. G., & Zuber, M. T., 2013. The Crust of the Moon as Seen by GRAIL, *Science*, **339**(6120), 671–675.

Wieczorek, M. A., Meschede, M., Sales de Andrade, E., Oshchepkov, I., Xu, B., & Walker, A., 2018. SHTOOLS: Version 4.3, Zenodo.